Journal of the European Ceramic Society **18** (1998) 329–338

PII: S0955-2219(97)00137-4
0955-2219/98/$19.00 + 0.00

Strength Predictions for Notched Alumina Specimens

D. Hertel,* T. Fett and D. Munz

Universität Karlsruhe, Institut für Zuverlässigkeit und Schadenskunde im Maschinenbau, und Forschungszentrum Karlsruhe, Institut für Materialforschung II, Postfach 3640, D-76021 Karlsruhe, Germany

(Received 26 March 1997; accepted 3 July 1997)

Abstract

Ceramics fail in most cases by unstable extension of natural defects. Whilst strength measurements are mostly available for simple test specimens, it is of practical interest to develop procedures which allow to predict the strengths of more complicated components. Several possibilities are considered which are based on a principal stress criterion, a fracture mechanics procedure using single cracks (including stress gradients and R-curve behaviour), and on a procedure which applies multiaxial Weibull statistics to the surface and volume defect population. © 1998 Published by Elsevier Science Limited.

1 Introduction

Failure of ceramic components is caused by unstable extension of natural crack-like defects, which are always present due to manufacturing and surface treatment. Whilst the failure behaviour has been studied in the literature mostly for simple components (e.g. rectangular bending bars), combined with uniaxial stress states, real components are of a more complex structure and in a multiaxial stress state. As an example of such a component the notched bending bar will be considered in this investigation.

In the most general case of multiaxial stress state failure can be assessed using the multiaxial Weibull theory. Therefore, it is assumed that the component contains flaws of random size, of random location and of random orientation with respect to the principal stress axes. Theoretical considerations for notched components were made by Brückner-Foit *et al.*[1] Experimental results can hardly be found in the open literature. Strength results without theoretical analysis were given by Wang *et al.* [2]

The aim of this paper is to predict the strength of notched bars with different notch root radii from the strength of flat unnotched bars and to compare these predictions with strength measurements.

2 Failure of Notched Bars

2.1 Failure probability under multiaxial stresses

The fracture by unstable propagation of natural flaws leads to a scatter behaviour of strength data which reflects the scatter in flaw sizes and locations. The basis for the computation of the failure probability of a ceramic component is the multiaxial Weibull theory.[3–6] In the statistical treatment it is assumed that the flaws can be described by cracks which are randomly distributed with respect to their location and orientation. The most severest crack, given by the most serious combination of size, location and orientation, is responsible for fracture.

Following the analysis made by Brückner-Foit *et al.*[1] the failure probability P_f is given as:[3,5,6]

$$P_f = 1 - \exp\left[-\frac{1}{V_0}\int_{\Omega}\frac{1}{4\pi}\int_{V}\left(\frac{\sigma_{eq}}{\sigma_0}\right)^m \mathrm{d}V\mathrm{d}\Omega\right] \quad (1)$$

where σ_0 and m are the Weibull parameters, Ω is the surface of a unit sphere, and V_0 is a reference or unit volume. The equivalent stress σ_{eq} is a function of the principal stresses σ_1, σ_2 and σ_3 and the polar angles (α, β), which determine the crack plane relative to the principal axes. To calculate σ_{eq} we need the stress σ_n normal to the crack plane

$$\sigma_n = \left(\sigma_1 \cos^2\alpha + \sigma_2 \sin^2\alpha\right)\sin^2\beta + \sigma_3 \cos^2\beta \quad (2)$$

and the shear stress in the crack plane

*Now at ABB, Baden, Switzerland.

$$\tau = \sqrt{\tau_{r\alpha}^2 + \tau_{r\beta}^2} \tag{3}$$

with

$$\tau_{r\alpha} = (\sigma_2 - \sigma_1)\sin\alpha\cos\alpha\sin\beta \tag{4}$$

and

$$\tau_{r\beta} = \left(\sigma_1\cos^2\alpha + \sigma_2\sin^2\alpha - \sigma_3\right)\sin\beta\cos\beta \tag{5}$$

Different multiaxiality criteria are known in the literature (see e.g. Ref. 7). An often used criterion, based on the energy release rate in the crack plane is [8]

$$\sigma_{eq} = \sqrt{\sigma_n^2 + \left(\frac{2}{2-\nu}\right)^2\tau^2} \tag{6}$$

The failure probability may be expressed as a Weibull distribution with the parameters m and b

$$P_f = 1 - \exp\left[-\left(\frac{\sigma*}{b}\right)^m\right] \tag{7}$$

where $\sigma*$ is a reference stress, e.g. the maximum principal stress. The parameters b and H are defined by

$$b = \sigma_0 H^{-1} \tag{8}$$

and

$$H = \left[\frac{V_{eff}}{V_0}\right]^{\frac{1}{m}} = \left[\frac{1}{V_0}\int_\Omega \frac{1}{4\pi}\int_V \left(\frac{\sigma_{eq}}{\sigma*}\right)^m \mathrm{d}V\mathrm{d}\Omega\right]^{\frac{1}{m}} \tag{9}$$

where V_{eff} is the effective volume. In the preceding considerations only volume defects were taken into account. If surface cracks are responsible for failure, one obtains similar to eqn (1):

$$P_{f,A} = 1 - \exp\left[-\frac{1}{A_0}\frac{1}{2\pi}\int_0^{2\pi}\int_{(A)}\left(\frac{\sigma_{eq}}{\sigma_{0,A}}\right)^m \mathrm{d}A\mathrm{d}\alpha\right] \tag{10}$$

where A_0 is the unit surface. An H-value, given in eqn (9) for the volume, can also be defined for the effective surface.

2.1.1. Prediction of the component strength

The normalised effective volume H [eqn (9)] is independent of the height of the load $\sigma*$. Therefore, it is an appropriate tool to estimate the influence of a stress distribution on the failure probability. In this investigation the quantity is used to predict from a known geometry the failure probability for another geometry. The basis of the prediction is eqn (8). The quotient of the two Weibull parameters $b^{(1)}$ and $b^{(2)}$ for two geometries results as

$$\frac{b^{(1)}}{b^{(2)}} = \frac{H^{(2)}}{H^{(1)}} \tag{11}$$

The ratio of the allowed stresses is then

$$\frac{\sigma^{(1)*}}{\sigma^{(2)*}} = \frac{H^{(2)}}{H^{(1)}} \tag{12}$$

where $\sigma^{(1)*}$ and $\sigma^{(2)*}$ are the maximum admissible reference stresses for a certain failure probability P_f. The numerical value of H depends on the definition of the reference stress [see eqn (9)]. The strength predictions performed with eqn (12) are related to the reference stress defined by eqn (9). In case of a notched bar this stress may be the nominal (net section) stress σ_{nom} or the stress at the notch root σ_k, defined by

$$\sigma_k = K_t\sigma_{nom} \tag{13}$$

where K_t is the stress concentration factor. From eqn (8) the dependency between the Weibull parameters and the H-values results

$$\sigma_0 = b_{nom}H_{nom} = b_kH_k = K_tb_{nom}H_k \tag{14}$$

The H-values, consequently, differ by the factor K_t:

$$H_{nom} = K_tH_k \tag{15}$$

and for the strength predictions it holds

$$\frac{\sigma_{nom}^{(1)}}{\sigma_{nom}^{(2)}} = \frac{H_{nom}^{(2)}}{H_{nom}^{(1)}} = \frac{K_t^{(2)}H_k^{(2)}}{K_t^{(1)}H_k^{(1)}} \tag{16}$$

3 Numerical Computations

3.1 Stress concentration factors and stress intensity factors

For computation of failure stresses at the notch root from the experimentally determined bending

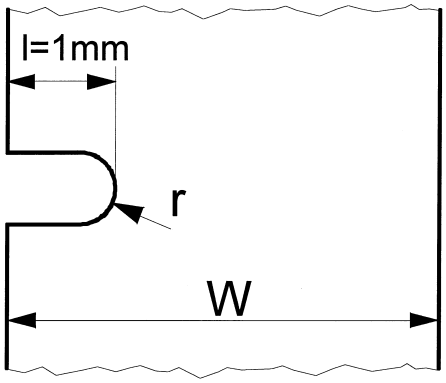

Fig. 1. Notch geometry (schematical).

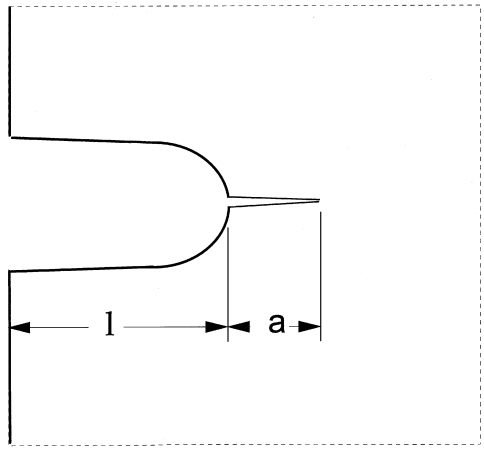

Fig. 2. Crack ahead of a circular notch.

moment we computed the stress concentration factors of the notch geometries using the Finite-Element Method (FEM) and the Boundary Element Method (BEM). The geometric data of the specimens with notches are illustrated in Fig. 1.

The FE-calculations were performed with ABAQUS,[9] and in case of the BEM analysis the BEASY 5·0 program system[10] was used. Plane stress conditions were assumed. The stress concentration factor is defined in eqn (13) with the notch root stress σ_k known from the numerical stress analysis. Table 1 shows the geometries used and the concentration factors obtained together with two results from the literature.[11] The results of the FEM-analysis and the BEM computation showed maximum differences less than 1%.

Stress intensity factors for cracks emanating at the notch root were computed with the BEM program package (BEASY Crack Growth)[12] using the *J*-integral method. The cracks were assumed as through-the-thickness cracks with the crack plane normal to the specimen length axis. The stress intensity factors were expressed by the geometric functions *Y* according to

$$K_1 = \sigma\sqrt{a+l}Y \tag{17}$$

where σ is the outer fibre bending stress, l is the notch length and a is the crack size (see Fig. 2).

The stress intensity factors—expressed by the geometric function—are shown in Fig. 3 (upper part) for the narrow notch and in the lower part for the wide notch. The crack length normalised to the notch root radius r is given by the upper scale. The figures additionally show the two well-known limit cases, namely the short-crack solution expressed by

$$K_{l,s} = 1{\cdot}12\sigma_k\sqrt{\pi a} \tag{18}$$

and the long-crack limit in which it is assumed that the crack-notch configuration acts as an edge-crack of total length $l+a$, with the geometric function taken from Ref. 13 In accordance with Ref. 14 slight overshooting is visible.

Table 1. Comparison of the stress concentration factors

Specimen geometry		*Stress concentration factor*		
Notch radius (mm)	*Cross-section B×W (mm)*	*FEM*	*BEM*	*Peterson (Ref. 11)*
0·05	3·0×4·0	5·88	5·88	—
0·8	3·0×4·0	1·78	1·78	1·75
0·05	3·5×4·5	6·26	6·26	—
0·8	3·5×4·5	1·89	1·89	1·82

3.2 Determination of the effective volumes

Strength predictions were performed using the software package STAU.[15] In this procedure first the stress distribution in the whole component is determined by FEM. The statistical data as the Weibull parameters are introduced and the failure criterion and the *H*-values are evaluated by numerical integration. For the computation of the *H*-values the specimen length 45mm and the normal 4-point-bending test arrangement (outer roller span 40mm, inner roller span 20mm) were used. The maximum principal stress in the component was used as the reference stress. In case of the notched bars the maximum stress at the notch root was applied and for the unnotched specimens the maximum outer fibre stress was used. We used the normal stress criterion as the failure criterion.[1,7]

The results are plotted in Fig. 4 for surface cracks (upper diagram) and for volume cracks (lower diagram) as a function of the Weibull exponent m. The *H*-values for the three geometries approach the same asymptotic limit for large Weibull exponents

$$\lim_{m\to\infty} H(m) = H^{<0{\cdot}05>} = H^{<0{\cdot}08>} = H^{<\infty>} \tag{19}$$

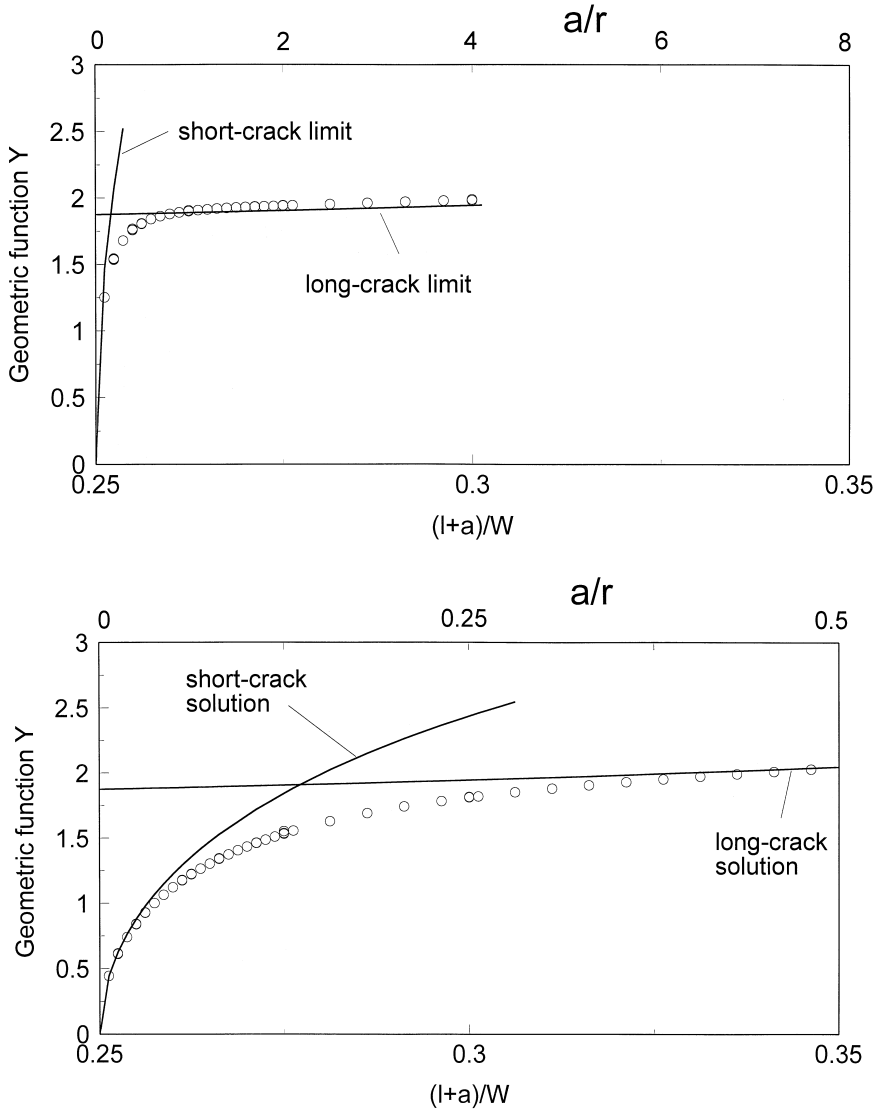

Fig. 3. Geometric function for a crack ahead of a notch (upper diagram: $r = 0{\cdot}05$ mm, lower diagram $r = 0{\cdot}8$ mm).

where the superscripts symbolise the notch radius and $<\infty>$ stands for the plane bar. The strength predictions then read according to eqn (12)

$$\lim_{m\to\infty} \sigma* = \sigma*_K^{<0{\cdot}05>} = \sigma*_K^{<0{\cdot}8>} = \sigma*_K^{<\infty>} \qquad (20)$$

This result means that in case of negligible scatter behaviour the strength of the component is determined only by the maximum stress occurring and the value of the effective volumes will not be important. With increasing scatter (decreasing m) the H-values differ more and more from each other and the failure stress at the notch root differs significantly.

4 Experimental Results

4.1 Bending strength

Two different aluminas were tested, a fine-grained 99·7% Al_2O_3 (Rk87, Cerasiv, Plochingen) with a mean grain size 2·5–3 μm, and a 99·6% Al_2O_3 (Al23, Friatec, Mannheim) with a mean grain size of 20 μm. The surfaces of the straight bars and the notches were finished with a diamond wheel D46 operating perpendicular to the specimen length axis. The strength measurements are shown in Fig. 5 for the fine-grained material (upper diagram) and for the coarse-grained alumina (lower diagram). While for the unnotched specimens the outer fibre bending stress is defined as the strength, we used in case of the notched bars the stress at the notch root as the strength values. In Table 2 the Weibull parameters obtained with the maximum likelihood procedure are entered together with the 90% confidence intervals (data in parentheses).

The comparison of the strength data shows that the narrow notches tolerate higher notch stresses than the wider ones. The lowest strength is found for the plane specimen with infinite notch root radius. For the Weibull exponents no significant differences are obvious for the fine-grained Rk87, but in case of the coarse-grained Al23 the m-values

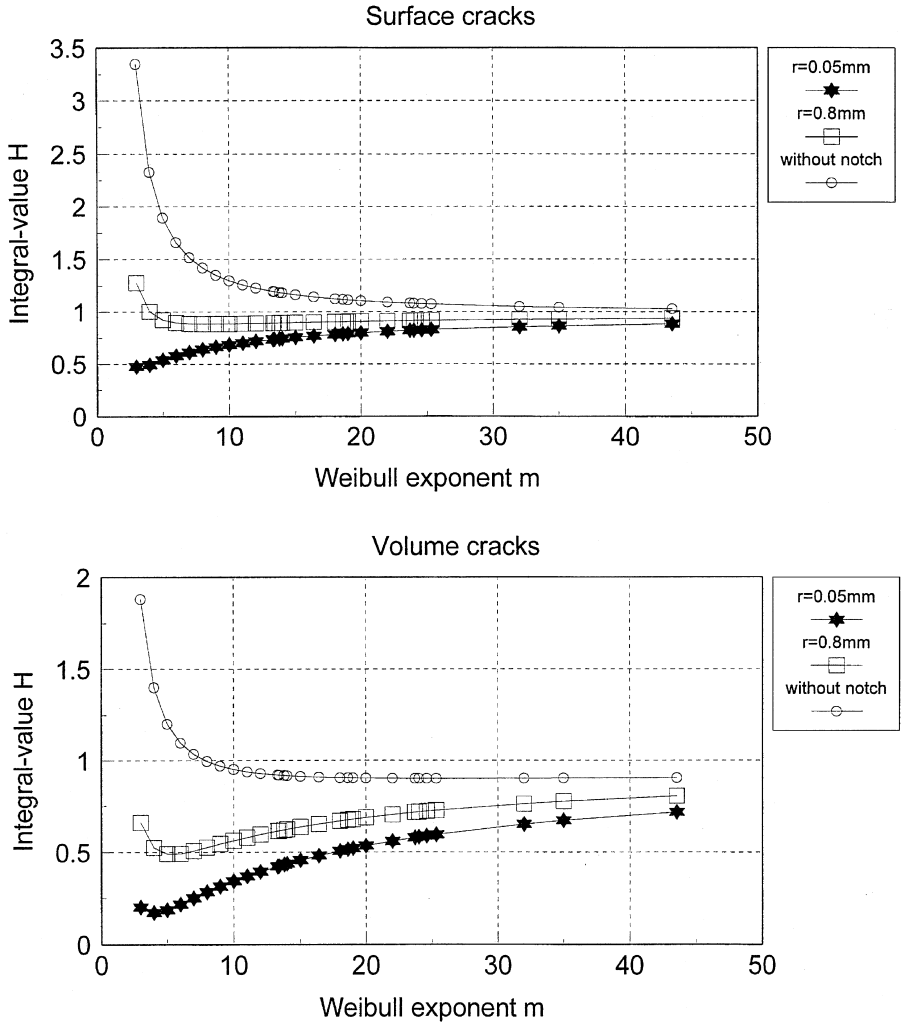

Fig. 4. *H*-values for notched and unnotched specimens; notch root radii r: 0·05 mm, 0·8 mm, and ∞. Specimen size $B \times W$: $3{\cdot}0 \times 4{\cdot}0\,\text{mm}^2$.

for notches (identical for the two radii) are significantly higher than for the unnotched bars.

4.2 Fracture toughness and R-curve

Fracture resistance measurements were carried out with SENB specimens in bending with an initial saw-cut of relative depth $a_0/W \cong 0{\cdot}5$ and a width of 50 μm. The *R*-curve was determined in a controlled fracture test using an extremely rigid 3-point-bending test device. The *R*-curves determined with the compliance method are shown in Fig. 6 for Rk87 and for Al23. The initial toughness values were determined in a series of tests as (mean value and standard deviation) to be

$$\bar{K}_{I0} = 3{\cdot}0 \pm 0{\cdot}29\ \text{MPa}\sqrt{m}$$

for (fine-grained) Rk87, and

$$\bar{K}_{I0} = 2{\cdot}4 \pm 0{\cdot}43\ \text{MPa}\sqrt{\text{m}}$$

for (coarse-grained) Al23.

5 Strength Predictions

5.1 Types of predictions

The strength can be predicted for different failure conditions. Five possibilities, abbreviated as methods (I) to (V), are outlined below, and three different predictions will be made, denoted, predictions A, B and C. Prediction A is a prediction from the plane bar to the narrow notch, prediction B is also based on the plane bar data and predicts the strength of the wide notch, and, finally, prediction C predicts the narrow notch strength from data of the wide notch. In principle, only two of these three possibilities are independent.

5.1.1. Maximum stress (I)

The simplest method of predicting strength is based on the criterion

$$\sigma_{max} = \sigma_c \tag{21}$$

Failure occurs when the maximum principal stress in the component reaches a critical value. The

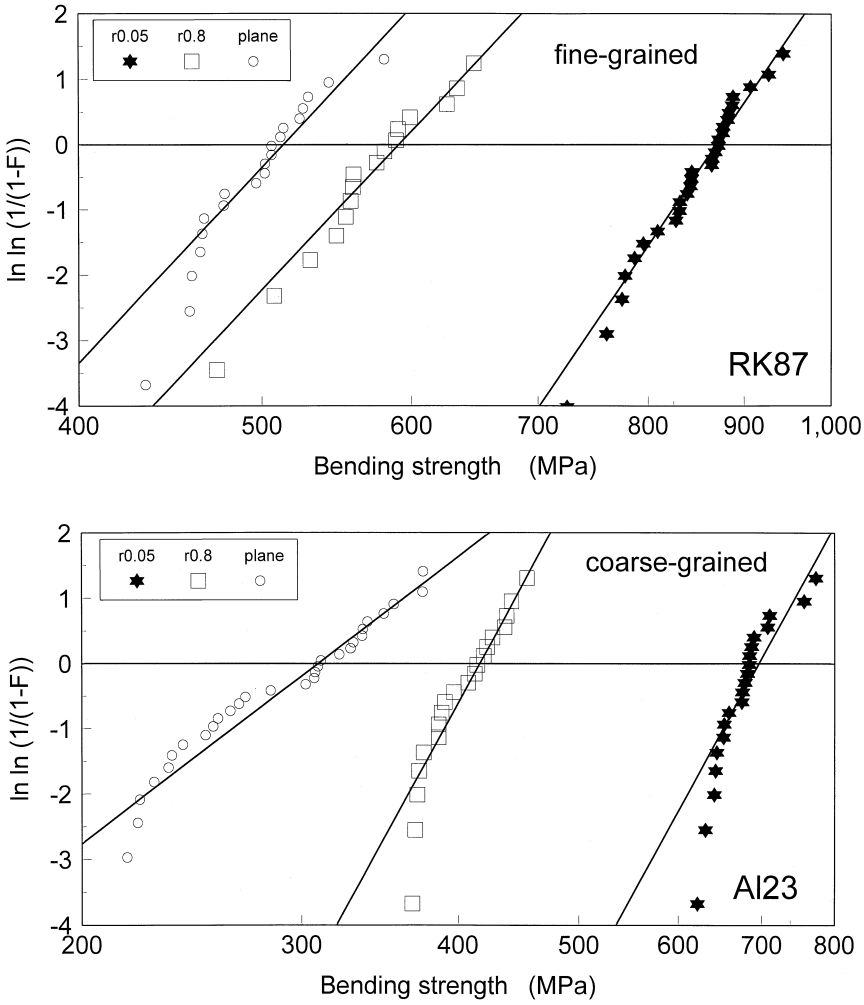

Fig. 5. Inert strength for notched and unnotched specimens. Upper diagram: fine-grained alumina. Lower diagram: coarse-grained alumina.

Table 2. Weibull-parameters of strength with 90%-confidence intervals (columns 2 and 3 Rk87, columns 4 and 5 Al23)

Notch radius	*Weibull-parameter* b*(MPa)*	*Weibull-exponent* m	*Weibull-parameter* b*(MPa)*	*Weibull-exponent* m
0·05mm	869·4 [854; 885]	18·6 [14·5; 24·0]	696·6 [679; 715]	15·1 [11·2; 20·5]
0·8mm	590·9 [572; 611]	13·3 [9·5; 18·8]	416·5 [406; 428]	15·2 [11·2; 20·6]
∞	513·5 [498; 529]	13·4 [9·9; 18·2]	309·3 [294; 326]	6·3 [5·0; 8·1]

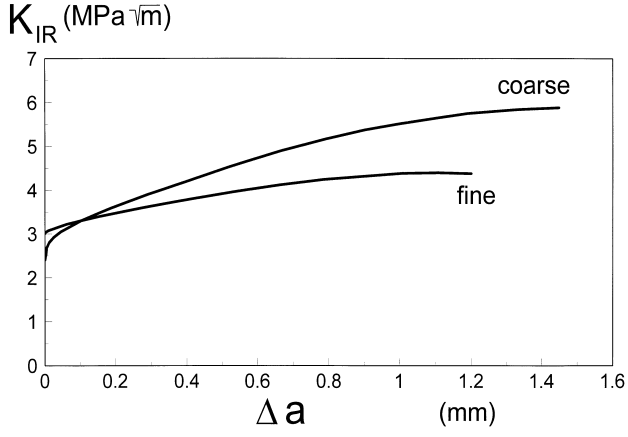

Fig. 6. *R*-curve for fine-grained Al_2O_3 (Rk87) and coarse-grained Al_2O_3 (Al23).

maximum principal stresses occur for the notched bars at the notch root and in case of the unnotched specimens at the outer fibre of the tensile region. If these reference stresses are used, one has to expect identical strength data for all geometries. In Fig. 7 the strength data predicted for the three possible directions of prediction are entered as vertical bars (I) for the Rk87 alumina and for the Al23 material. The deviations between prediction and experiment (represented by the horizontal scatter bands) are significant for both materials in case of predictions A and C.

5.1.2. Critical crack size without R-curve (II)

This method is based on the assumption that in case of all geometries comparable cracks are

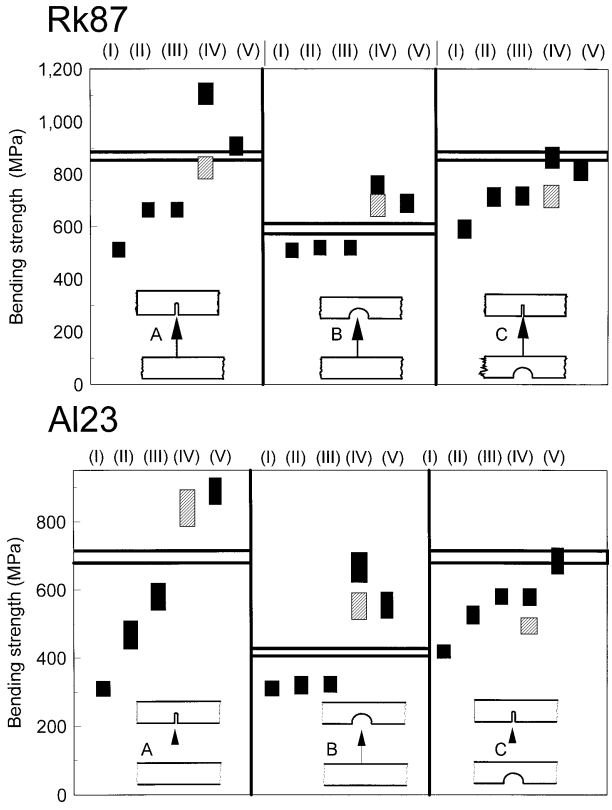

Fig. 7. Comparison of strengths with predictions for Rk87 and Al23. Predictions for 90% confidence. (I) Maximum stress; (II) critical crack length; (III) similar to (II), but with R-curve behaviour considered; (IV) Weibull statistic (black: volume cracks, grey: surface cracks); (V) critical crack length combined with reduced effective surface. Horizontal bars: scatter band of easured bending strength. 'Bending strength' defined as the maximum principal stress at the notch root.

responsible for failure, i.e. it is assumed that machining a notch causes the same flaw population as machining the plane surfaces. In this approximation the increase in the crack resistance curve is ignored and failure is described by the condition $K = K_{10}$. The size of such a crack (described by a through-the-thickness crack) is derived from the strength of the geometry '1', the strength of the unnotched bar

$$a_c = \left(\frac{K_{10}}{\sigma_c^{(1)}\, Y^{(1)}}\right)^2, \sigma_c^{(2)} = \frac{K_{10}}{\sqrt{a_c}\, Y^{(2)}} = \sigma_c^{(1)} \frac{Y^{(1)}}{Y^{(2)}} \quad (22)$$

Table 3. Strength prediction for fine-grained alumina (RK87) using method (II)

Notch geometry	*Experiment* b *(MPa)*	a_c *(μm)*	*Y*	*Prediction* $\sigma_{k,pred}$ *(MPa)*
$r = \infty$	513·5	8·67	1·984	—
$r = 0{\cdot}8$ mm	—	8·67	1·956	520·3 B
$r = 0{\cdot}05$ mm	—	8·67	1·532	664·3 A
$r = 0{\cdot}8$ mm	590·9	6·64	1·970	—
$r = 0{\cdot}05$ mm	—	6·64	1·624	716·9 C

and the strength for geometry '2' is given by $\sigma^{(2)}{}_c$, with the geometric functions known from the numerical analysis. In contrast to method (I), this procedure takes into account the decreasing stress with increasing distance from the notch root.

Table 3 illustrates the prediction procedure in case of the fine-grained material. The predictions were made for $\sigma_c = b$, i.e. for a failure probability $F = 0{\cdot}632$. Starting with the strength of the unnotched specimens, the fracture toughness and the geometric function for edge cracks, the critical crack length for the unnotched specimens $a_c{}^{\infty}$ is computed with eqn (22). Assuming that this crack size is also typical of the notched specimens, i.e.

$$a_c^{<r=0{\cdot}05>} = a_c^{<r=0{\cdot}8>} = a_c^{<\infty>}$$

the prediction according to eqn (22) using the geometric functions for cracks at notch roots provides the strength data entered in the last column of Table 3.

In Fig. 7 the predictions (marked II) are compared with the experimental data. This type of prediction gives strengths which are by about 20% below the experimental results for predictions A and C, but are in good agreement with the experimental findings in case of prediction B. Figure 7 shows the same type of prediction also for the coarse-grained material Al23.

5.1.3. Critical crack length with R-curve effect (III)
This procedure is similar to method (II). But in this case the effect of the *R*-curve is taken into consideration. The failure stress results from the tangent condition between the applied stress intensity factor as the loading quantity, the $K_{I,appl}$-a-curve, and the crack resistance curve K_{IR}

$$K_{I,appl} = K_{IR} \quad (23)$$

$$\left(\frac{\partial K_{l,appl}}{\partial a}\right)_{\sigma=const=\sigma_c} = \left(\frac{dK_{IR}}{da}\right) \quad (24)$$

In case of the less pronounced *R*-curve behaviour of Rk87, the condition of instability is fulfilled only by eqn (23), and a tangent condition according to eqn (24) does not exist. Consequently, failure occurs at $a = a_i$ and the initial value of the K_I-*a*-curve, i.e. K_{I0}, has to be used. The principal treatment is identical with method (II) and, consequently, the same predictions result for methods (II) and (III). In case of the coarse-grained Al23 with its strongly increasing *R*-curve methods (II)

and (III) give different results. The predictions are entered in Fig. 7 as result (III).

5.1.4. Prediction using effective volumes or effective surface (IV)

This method is based on the statistical assessment of failure probabilities. For the strength prediction from one geometry (1) to the other (2) it results from eqn (12):

$$\sigma^{(2)*} = \sigma^{(1)*} \frac{H^{(1)}}{H^{(2)}} = \sigma^{(1)*} \frac{b^{(2)}}{b^{(1)}} \tag{25}$$

where $\sigma^{(1)*}$ and $\sigma^{(2)*}$ are the maximum allowable reference stresses for the component geometries and $H^{(1)}$ and $H^{(2)}$ are the normalised effective volumes or surfaces. The H-values for the considered specimens are known from the numerical computations, presented in Section 3. Figure 8 shows the H-ratios for the combinations A, B and C as a function of the Weibull exponent m for the assumptions of volume or surface defects. If the type of defect population is known (volume or surface cracks), the ratio of the predicted strengths results as the reciprocal of the H-value ratio—see eqn (25). If prediction and experiment agree, the ratio of the H-values must correspond to the reciprocal ratio of the experimentally determined Weibull parameters b. In order to check this, the ratio of b-values is additionally plotted versus the experimental Weibull exponents m (90% confidence intervals used) which results in the horizontal bars. The related geometries (1) and (2) are illustrated by the inserts in Fig. 8.

A statistical compatibility of prediction and experiment can be stated if the curves for the H-ratios intersect the horizontal bars. Since the type of failure relevant defects could not be identified definitely by fractography, the compatibility has to be discussed separately for volume cracks as well as for surface cracks. The procedure is very simple in cases where the Weibull exponents in the notched and unnotched specimens are identical. A complication occurs if the m-values are different from each other. Therefore, two different horizontal bars have to be considered. The solid one results, if b-ratio is plotted versus the confidence interval of Weibull parameter $m^{(1)}$ of geometry (1) and the dashed one if b-ratio is plotted versus the m-confidence interval of geometry (2). In order to improve the recognition, the two bars are plotted at slightly different b-ratios.

For Rk87 all Weibull exponents are nearly identical. In case of specimen combination A the m confidence interval for the notched bars is slightly shifted to higher values compared with the unnotched bars. The degree of compatibility depends on the chosen confidence interval. If we choose the interval corresponding to the unnotched specimens, an agreement can be stated for surface cracks only. In case of the notched specimens a better agreement is obtained for the volume defects. Specimen combination B shows complete overlapping of the confidence intervals. But in this case no agreement between prediction and measurement can be seen. The prediction C shows an agreement for volume cracks. From the results of Fig. 8 we can summarise that no clear statement can be made about the failure- relevant defect population. Finally, it should be mentioned that the inverse predictions from (2) to (1) results in the same diagram since only the ratios of H-values enter Fig. 8.

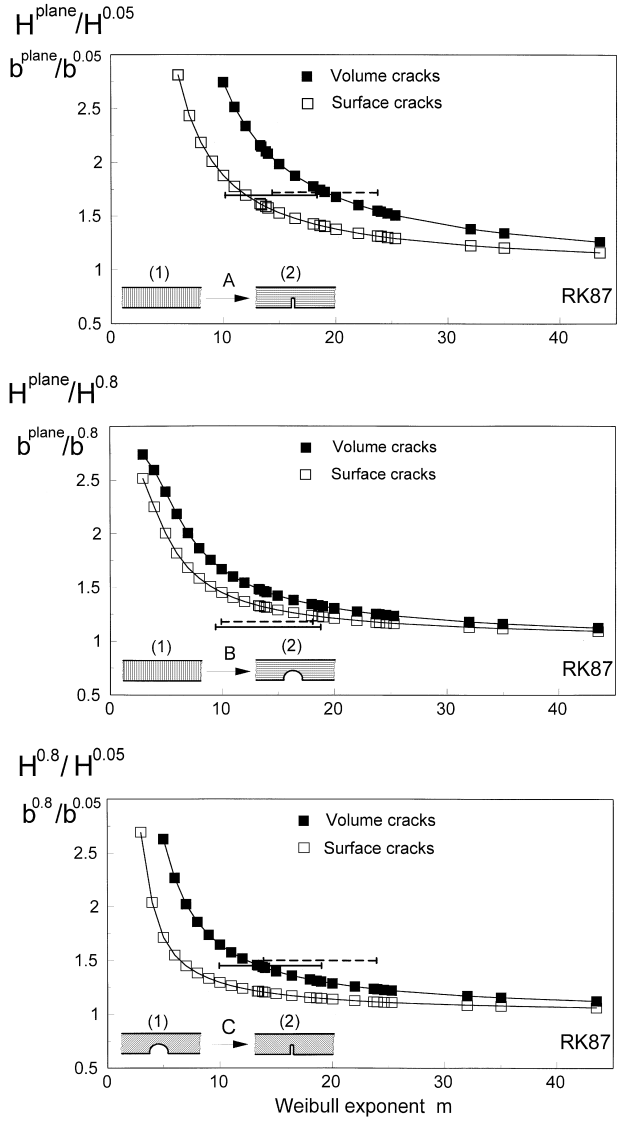

Fig. 8. Comparison of the H-values with the Weibull parameters of the bending strength (Rk87). Symbols: H-ratios. Horizontal bars: b-ratios, plotted versus the 90%-confidence intervals of Weibull parameter m. Solid bar: based on Weibull parameter for geometry (1); dashed bar: based on Weibull parameter for geometry (2).

5.1.5. Combination of effective surface and single crack behaviour (V)

In method (II) it was assumed that the single crack at the notch root exhibits the same absolute size as the failure relevant crack (with crack size $a_c^{(1)}$) in the surface of the plane bar ignoring all statistical effects. In procedure (V) the reduced effective surface near the notch root is taken into consideration. The corresponding crack size $a_c^{(2)}$ results from eqns (8) and (22)

$$a_c^{(2)} = a_c^{(1)} \left(\frac{H^{(2)}}{H^{(1)}} \right)^2 \leq a_c^{(1)} \tag{26}$$

From this crack length the new geometric function $Y^{(2)}$ can be computed and the strength $\sigma_c^{(2)}$ of the notched bar results as

$$\sigma_c^{(2)*} = \sigma_c^{(1)} \frac{H^{(1)}}{H^{(2)}} = \frac{Y^{(1)}}{Y^{(2)}} \tag{27}$$

More details of this procedure will be published in a separate paper.[16]

5.2 Discussion of the predictions

In Fig. 7 the predictions are compared for the five different methods. The upper illustration relates to the fine-grained alumina, the lower one to the coarse-grained material. The confidence intervals of the predictions are represented by vertical bars. The experiments are shown by the horizontal lines which represent the scatter of strength data. In the special case of the Weibull evaluation the solid vertical bars relate to volume cracks, the shaded bars to surface cracks. Here the Weibull exponent of the flat bar was used for predictions 'A' and 'B', and in prediction 'C' the Weibull exponent of the bars with wide notch was applied. There is no specific case where an agreement between prediction and experiment was found for all three specimen combinations and for the two materials. The prediction method (I) obviously yields the poorest results in all cases. The best results are found with the Weibull procedure (method IV) and with the combination procedure (V).

In case of Rk87 the predictions 'A' and 'B' agree excellently under the assumption that surface cracks dominate failure, whereas prediction 'C' can be described slightly better on the basis of a volume crack population.

In case of Al23 the single-crack description, including *R*-curve behaviour, gives the best agreement with the experiments. Similar agreement is found in cases 'A' and 'B' for the Weibull estimation with surface cracks and in case of 'C' using volume cracks. Summarising, we have to admit that all predictions are not sufficient for this material.

6 Summary

Different procedures for strength predictions are applied to differently notched bending bars.

1. Method (I) assumes that the maximum principal stress at the notch root governs failure.
2. Method (II) is based on the stress intensity for a single crack at the notch root, ignoring *R*-curve influences. In contrast to method (I), this procedure takes into account decreasing stress with increasing distance from the notch root.
3. Method (III) extends method (II) considering the *R*-curve behaviour.
4. Method (IV) applies the multiaxial Weibull statistics to the complicate stress state of the notched specimens. Volume cracks and surface cracks are distinguished in the prediction procedure.
5. Method (V) considers a single crack at the notch root with reduced size according to the reduced effective surface.

The predictions were compared with measurements carried out for two different aluminas. The best agreement between strength prediction and strength measurement was found for the fine-grained alumina with method (IV) and (V) and for the coarse-grained alumina with method (III) and method (IV).

In case of the coarse-grained Al_2O_3 the Weibull modulus *m* for notched specimens was found to be significantly larger than that determined for unnotched specimens. The disagreement of the *m*-values, making the Weibull prediction problematic for the coarse-grained material, remains uninterpreted. One possibility may be that the machining procedure causes different flaw populations although identical diamond wheels (D46) and identical machining direction were ensured.

In addition to the strength also cyclic fatigue behaviour of the notched aluminas was studied in.[17]

References

1. Brückner-Foit, A., Heger, A. and Munz, D., On the contribution of notches to the failure probability of ceramic components. *J. Europ. Ceram. Soc.*, 1996, **16**, 1027–1034.
2. Wang, F., Zheng, X. L. and Lu, M. X., Notch strength of ceramics and statistical analysis. *Engng Fract. Mech.*, 1995, **52**, 917–921.

3. Batdorf, S. B. and Crose, J. G., A statistical theory for the fracture of brittle structures subjected to nonuniform polyaxial stresses. *J. Appl. Mech*., 1974, **41**, 459–461.
4. Batdorf, S. B. and Heinisch, H. L., Weakest link theory reformulated for arbitrary fracture criterion. *J. Am. Ceram. Soc*., 1978, **61**, 355–358
5. Evans, A. G., A general approach for the statistical analysis of multiaxial fracture. *J. Am. Ceram. Soc*., 1978, **61**, 302–308.
6. Matsuo, Y., A probabilistic analysis of the fracture loci under bi-axial stress state. *Bull. JSME*, 1981, **24**, 290–294.
7. Thiemeier, T., Brückner-Foit, A. and Kölker, H., Influence of the fracture criteria on the failure prediction of ceramics loaded in biaxial flexure. *J. Am. Ceram. Soc*., 1991, **74**, 48–52.
8. Paris, P. C. and Sih, G. C., *Stress analysis of cracks*. In: *Fracture Toughness Testing and its Applications*, pp. 30–83. ASTM STP 381, American Society of Testing of Materials, Philadelphia, PA, 1965.
9. *ABAQUS User's Manual*. Hibbitt, Karlsson, Sörensen INC., Version 4.8, 1989.
10. *Beasy 5.0, User Guide*. Computational Mechanics Publications, Southampton UK and Boston USA.
11. Peterson, R. E. *Stress Concentration Factors*. John Wiley Publications, New York, 1974.
12. *Beasy 5.0, Crack Growth Guidebook*. Computational Mechanics Publications, Southampton UK and Boston USA, 1994.
13. Srawley, J. E. and Gross, B., Side-cracked plates subject to combined direct and bending forces. pp.559–579. ASTM STP 601, 1976.
14. Fett, T., The stress intensity factor for small cracks at the root of a notch. *Int. J. Fract*., 1992, **54**, R57.
15. Heger, A., Bewertung der Zuverlässigkeit mehrachsig belasteter keramischer Bauteile. *VDI-Bericht 18*, 132, 1993.
16. Fett, T., Hertel, D. and Munz, D., Bending strength of notched bars. Submitted.
17. Hertel, D., Fett, T. and Munz, D., Fatigue of notched alumina specimens. In *Fracture Mechanics of Ceramics*, Vol. 12. Plenum Press, New York, 1996, 31–44.